Sensors and Materials, Vol. 34, No. 3 (2022) 1191–1201
MYU Tokyo

S & M 2882

Adaptive Speed Estimation with Genetic Algorithm for Vector-controlled Permanent Magnet Synchronous Motor Drive

Yung-Chang Luo,* Song-Yi Xie, Chia-Hung Lin, and Ying-Piao Kuo

Department of Electrical Engineering, National Chin-Yi University of Technology,
No. 57, Sec. 2, Zhongshan Rd, Taiping Dist., Taichung 41170, Taiwan (ROC)

(Received June 21, 2021; accepted September 8, 2021)

Keywords: vector-controlled (VC), permanent magnet synchronous motor (PMSM) drive, speed estimation, model reference adaptive system (MRAS), genetic algorithm (GA)

An adaptive speed estimation scheme was established for a vector-controlled (VC) permanent magnet synchronous motor (PMSM) drive. The current and voltage of the stator were used to develop a decoupling VC PMSM drive, and the speed, d-axis, and q-axis stator current control loops were designed using the linear PMSM mathematical model. Hall effect current sensors were used to measure the current of the PMSM. A model reference adaptive system (MRAS) was used to develop a speed estimation scheme based on the reactive power of the PMSM. The pole placement was used to design the d-axis and q-axis stator current controllers, and the speed controller was designed using the genetic algorithm (GA). The MATLAB/Simulink® toolbox was used to establish the simulation scheme, and all the control algorithms were realized by a microprocesser control card. Simulation and experimental results (including the estimated rotor speed, stator current, estimated electromagnetic torque, stator flux position angle, and stator flux locus) confirmed the effectiveness of the proposed approach.

1. Introduction

The development of sustainable and smart electric machine tools requires high-efficiency drives. As permanent magnet synchronous motors (PMSMs) only have high-permeability permanent magnets on the rotor without winding copper losses, they are widely used in today's factories to actuate appliances. The time-varying and coupling mathematical model for the control of a PMSM is more difficult to derive than that for a DC motor. According to the vector-controlled (VC) theory of AC motors,[1] by coordinate transformation, the complicated mathematical model of a PMSM is divided into the flux-current and torque-current components. These components are orthogonal and can be controlled independently. This is analogous to a separately excited DC motor, and the maximum torque-to-current ratio is attained. Conventional VC PMSM drives require a rotor position sensor such as an encoder to detect the shaft position. However, this sensor reduces the robustness of the PMSM drive and is unsuitable for hostile environments. Hence, the development of speed estimation techniques in place of this speed

*Corresponding author: e-mail: luoyc@ncut.edu.tw
https://doi.org/10.18494/SAM3480

ISSN 0914-4935

sensor is required for VC PMSM drives. Several speed estimation methods for a VC PMSM drive have been published: speed adjustment through the flux observer or the electromotive force of a PMSM,[2–5] speed determination using a neural network or fuzzy logic control,[6–9] speed estimation from an extended Kalman filter,[10–13] and speed identification via an adaptive control theory.[14–17] In this study, an adaptive speed estimation scheme was developed for a model reference adaptive system (MRAS) that was based on the reactive power of a PMSM. The speed controller of the proposed VC MRAS PMSM drive was designed using the genetic algorithm (GA). Electromagnetic Hall effect currents were used to detect the stator current for the implementation of the adaptive speed estimation scheme.

This paper is composed of six sections. Section 1 presents the research motivation, background, and literature review on speed estimation methods for VC PMSM drives. In Sect. 2. the decoupled VC PMSM drive design strategy is described. In Sect. 3, the MRAS speed estimation scheme based on the reactive power of a PMSM is discussed. Section 4 shows the design of the speed controller using GA in detail. Sections 5 and 6 cover the experimental setup and results, discussion, and conclusions.

2. Decoupling VC PMSM Drive

We assume that permanent magnets are arranged on the surface of a rotor without damping winding and that the magnetic axis of the permanent magnet is consistent with the d-axis of the rotor shaft. The stator voltage vector equation of a PMSM in the synchronous reference coordinate frame is given by[18]

$$R_s\vec{i}_s^{\,e} + \frac{1}{\omega_e}X_s p\vec{i}_s^{\,e} + jX_s\vec{i}_s^{\,e} + j\omega_e\lambda_F = \vec{v}_s^{\,e}, \tag{1}$$

where j stands for the imaginary part and $\vec{i}_s^{\,e} = i_{ds}^e + ji_{qs}^e$ and $\vec{v}_s^{\,e} = v_{ds}^e + jv_{qs}^e$ are the current and voltage vectors of the stator, respectively. Moreover, R_s and X_s are the resistance and reactance of the stator, respectively, λ_F is the equivalent rotor magnet flux linkage produced by the permanent magnet of the rotor, ω_e is speed of the synchronous reference coordinate frame, and $p = d/dt$ is the differential operator.

From Eq. (1), the d-axis and q-axis stator current state equations are derived as

$$pi_{ds}^e = -(\omega_e R_s / X_s)i_{ds}^e + (\omega_e / X_s)(v_{ds}^e + X_s i_{qs}^e), \tag{2}$$

$$pi_{qs}^e = -(\omega_e R_s / X_s)i_{qs}^e + (\omega_e / X_s)(v_{qs}^e - X_s i_{ds}^e - \omega_e\lambda_F). \tag{3}$$

Equation (2) shows that the third term on the right side is a coupling component associated with the q-axis stator current. Additionally, Eq. (3) shows that the third and fourth terms on the right side are the coupling components in relation to the d-axis stator current and rotor magnet flux

linkage, respectively. These coupling components permit the definition of the d-axis and q-axis stator voltage feedforward compensations as

$$v_{ds\_comp}^{e} = -X_s i_{qs}^{e}, \tag{4}$$

$$v_{qs\_comp}^{e} = X_s i_{ds}^{e} + \omega_e \lambda_F. \tag{5}$$

Hence, the linear control of the d-axis and q-axis stator current loops is achieved. The voltage commands of the d-axis and q-axis stator current control loops are obtained from

$$v_{ds}^{e*} = (\omega_e / X_s)(v'_{ds} + v_{ds\_comp}^{e}), \tag{6}$$

$$v_{qs}^{e*} = (\omega_e / X_s)(v'_{qs} + v_{qs\_comp}^{e}), \tag{7}$$

where v'_{ds} and v'_{qs} are the outputs of the d-axis and q-axis stator current controllers, respectively.

The generated electromagnetic torque of a PMSM is derived as

$$T_e = (P/2)\lambda_F i_{qs}^{e}, \tag{8}$$

where P represents the motor pole number. Equation (8) indicates that the equivalent rotor magnet flux linkage λ_F and the q-axis stator current i_{qs}^{e} are orthogonal, and the maximum torque-to-current ratio is inherent for a PMSM. The electromagnetic torque is controlled by the q-axis stator current. The mechanical equation of the motor is obtained as

$$J_m p\omega_{rm} + B_m \omega_{rm} + T_L = T_e, \tag{9}$$

where J_m and B_m are the motor inertia and viscous friction coefficient, respectively, T_L is the load torque, $\omega_{rm} = (2/P)\omega_r$ is the mechanical speed of the motor rotor shaft, and ω_r is the electric speed of the rotor.

Using Eqs. (2)–(5), the plant transfer functions of the d-axis and q-axis stator current control loops are respectively given as

$$G_{p\_i_{ds}}(s) = \frac{1}{s + \omega_e R_s / X_s}, \tag{10}$$

$$G_{p\_i_{qs}}(s) = \frac{1}{s + \omega_e R_s / X_s}. \tag{11}$$

Since the bandwidth of the inner q-axis stator current control loop is much higher than that of the outer speed control loop, the closed-loop gain of the q-axis stator current control loop can be regarded as unity. From Eq. (9), the plant transfer function of the speed control loop is given as

$$G_{p\_speed}(s) = \frac{1/J_m}{s + B_m/J_m}. \tag{12}$$

The linear control block diagram of the VC PMSM is shown in Fig. 1. The parameter pairs (K_{ps}, K_{is}), (K_{pd}, K_{id}), and (K_{pq}, K_{iq}) are the proportional and integral gains of the speed controller and d-axis and q-axis stator current controllers, respectively. As the rotor flux linkage is a permanent magnet, the d-axis stator current command has a value of 0. Here, the d-axis and q-axis stator current controllers were designed using the pole placement, and the speed controller was designed using GA.

3. MRAS Speed Identification Scheme Based on Reactive Power of PMSM

According to Eq. (1), the d-axis and q-axis stator voltage components can respectively be expressed as

$$v_{ds}^e = (R_s + (X_s/\omega_e)p)i_{ds}^e - \omega_e X_s i_{qs}^e, \tag{13}$$

$$v_{qs}^e = (R_s + (X_s/\omega_e)p)i_{qs}^e + \omega_e X_s i_{ds}^e + \omega_e \lambda_F. \tag{14}$$

The reactive power of a PMSM that is absorbed from the power source is given by

$$Q = v_{qs}^e i_{ds}^e - v_{ds}^e i_{qs}^e. \tag{15}$$

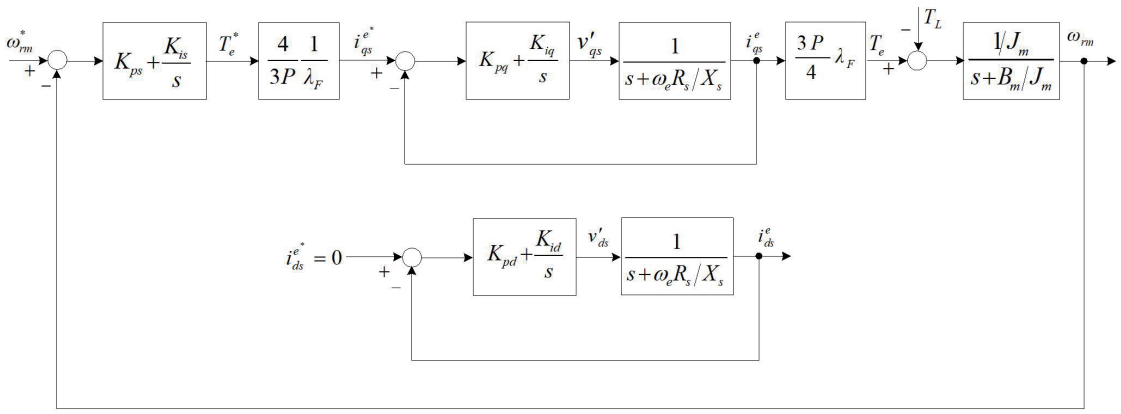

Fig. 1. Block diagram of linear control VC PMSM drive.

Under the VC condition, we substitute Eqs. (13) and (14) into Eq. (15), and the reactive power of a PMSM is expressed as

$$Q' = \hat{\omega}_e[(X_s/\omega_e)(i_{ds}^e)^2 + \lambda_F i_{ds}^e + (X_s/\omega_e)(i_{qs}^e)^2], \tag{16}$$

where "∧" implies an identified value. In MRAS theory,[19] Eq. (15) does not include the identified variable $\hat{\omega}_e$ to be selected as the reference model, and Eq. (16) is selected as an adjustable model because it contains $\hat{\omega}_e$. The difference between the reference model and the adjustable model is applied to an adaptation mechanism to adjust the identified synchronous speed $\hat{\omega}_e$. The synchronous position angle for the coordinate transformation between the two-axis synchronous coordinate frame and the three-phase system ($2^e \Rightarrow 3$ and $2^e \Leftarrow 3$) is obtained as

$$\hat{\theta}_e = \int \hat{\omega}_e dt. \tag{17}$$

The proposed MRAS speed identification scheme based on the reactive power of a PMSM is shown in Fig. 2.

4. Speed Controller Design Using GA

GA was used to design the speed controller of the proposed MRAS VC PMSM drive based on the reactive power. GA is one of the intelligent control methods based on Darwin's theory of evolution.[20,21] GA uses copulation to simulate natural selection and the survival of the fittest, wherein the more adaptable genes are retained and the less adaptable ones are eliminated, until the best value is obtained. GA generates the first generation (initial ethnic group) in a random manner. After a series of repeated natural selection, copulation, mutation, and elite processes, the optimized value is obtained.

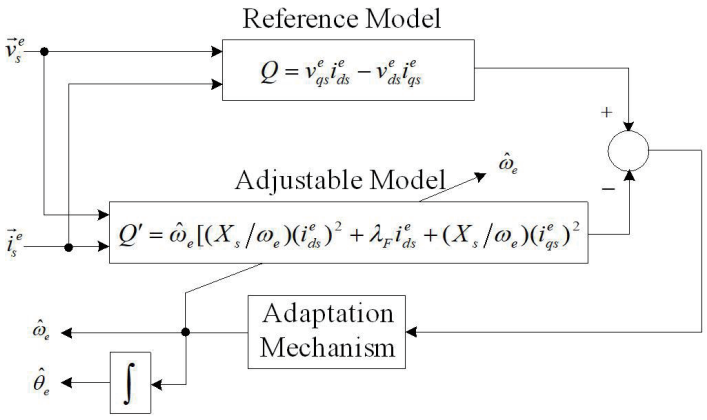

Fig. 2. MRAS rotor speed identification scheme based on the reactive power.

4.1 Natural selection

The natural selection operation retains better genes and eliminates unsuitable genes as shown in Fig. 3. The better adaptive genes are retained for continuous mating and mutation operations (upper figure), while the poorer adaptable genes are eliminated (lower figure).

4.2 Copulation

The copulation operation randomly selects a center point, and two chromosomes are exchanged to generate a new gene as shown in Fig. 4. The higher the rate of copulation, the more new offspring will be produced, and the best solution will be quickly determined. However, if the copulation rate is very high, excellent genes will be replaced because of continuous copulation. For this research, the copulation rate was set to 0.7.

4.3 Mutation

Adding mutations can prevent the mother gene from producing different chromosomes under the same conditions. The mutation operation will generate a mutation at a random point, and the lower mutation rate can avoid the loss of good genes as shown in Fig. 5. However, an excessively high mutation rate leads to random searches and loses the features. For this research, the mutation rate was set to 0.04.

4.4 Elite policy

In the mother generation, the excellent adaptation genes will be preserved and will not go through copulation and mutation, thus ensuring that these genes will not disappear and will be passed to future generations as shown in Fig. 6.

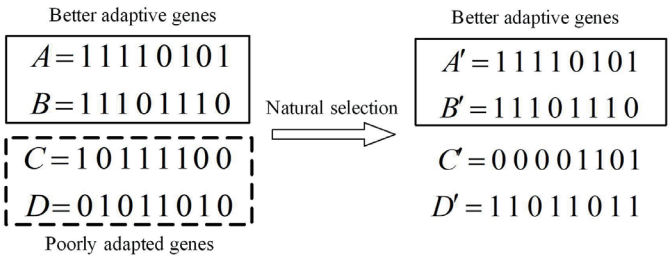

Fig. 3. Natural selection operation.

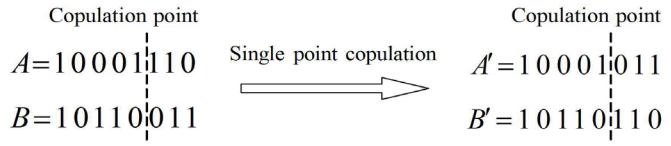

Fig. 4. Copulation operation.

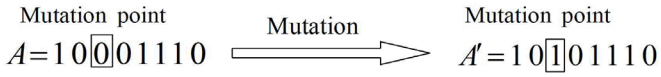

Fig. 5. Mutation operation.

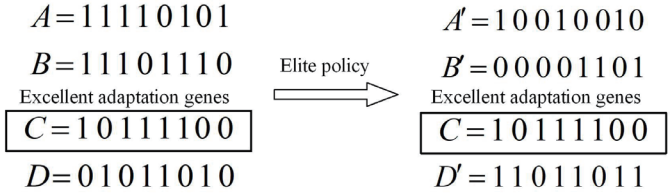

Fig. 6. Elite policy operation.

4.5 Fitness function

The fitness function determines whether a gene is the best solution. Then, the more adaptive genes will be retained and the less adaptive genes will be quickly eliminated. The fitness function is given by

$$f = \int_0^\infty te^2(t)dt, \tag{18}$$

where $e(t)$ is the error signal. The selected fitness function can obtain rapid convergence and good response.

The flow chart of the proposed GA is shown in Fig. 7. N new species are randomly generated from the initial population. The reproduction process selects the qualifying species on the basis of the fitness function value; those with higher values enter the copulation pool. Natural selection, copulation, and mutation continue iteratively until the set requirements are met, and the best value is obtained.

The block diagram of the proposed VC adaptive PMSM drive using GA is shown in Fig. 8, which includes a speed controller, d-axis and q-axis stator current controllers, d-axis and q-axis stator voltage decoupling, a two-axis synchronous frame to three-phase system coordinate transformation ($2^e \Rightarrow 3$), a three-phase system to two-axis synchronous frame coordinate transformation ($2^e \Leftarrow 3$), and an MRAS rotor speed identification scheme. In this system, the d-axis and q-axis stator current control loops are designed by the pole placement method. The speed controller is designed by GA. Hall effect current sensors are used as an electromagnetic sensing element to measure the three-phase stator current (dashed box in Fig. 8).

In this system, proportional–integral (P–I)-type controllers for the d-axis and q-axis stator current control loops are designed by the pole placement method. The speed control loop is designed using GA. The proportional gain (K_p), integral gain (K_i), damping ratio (ξ), undamped natural frequency (ω_n), and bandwidth (BW) for the two P–I-type controllers are shown in Table 1.

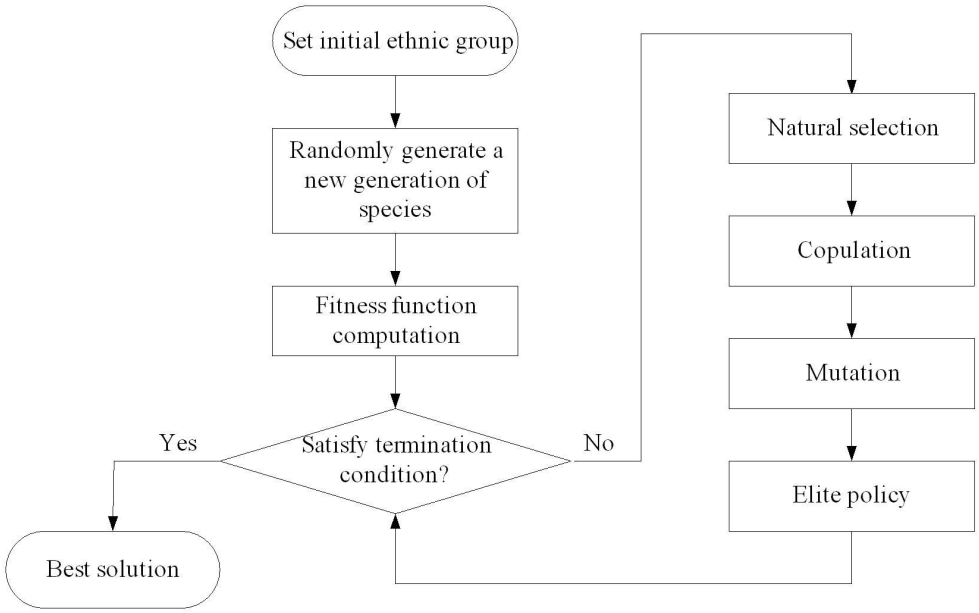

Fig. 7. Flow chart of the proposed GA.

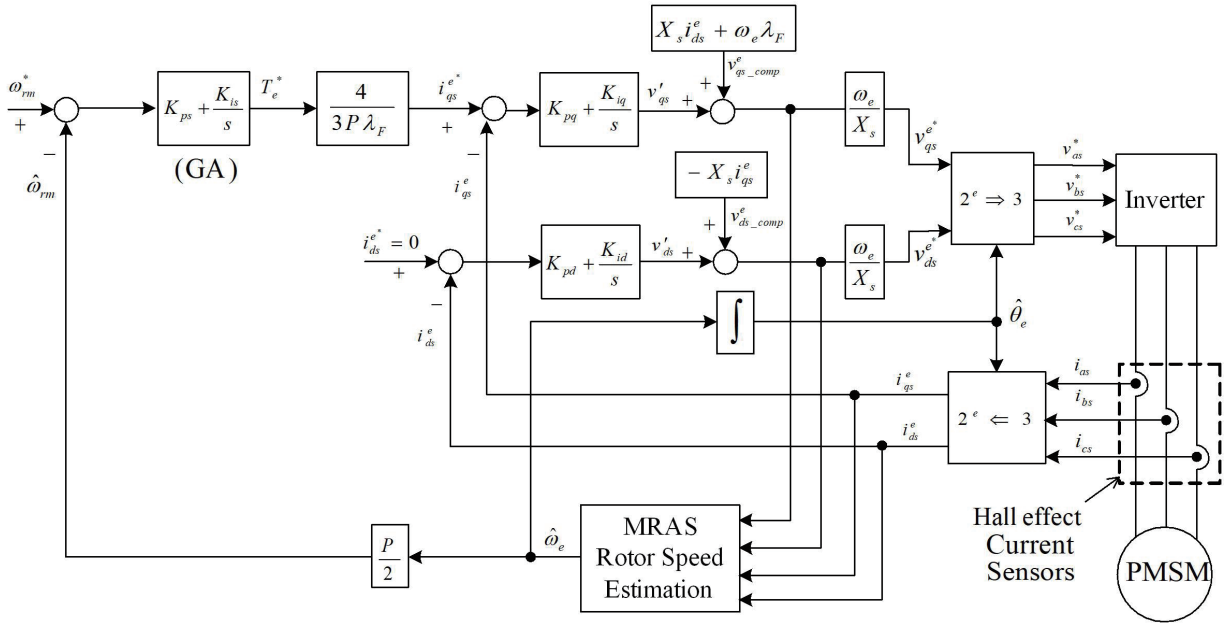

Fig. 8. VC MRAS PMSM drive using GA.

Table 1
Controller parameters, damping ratio, undamped natural frequency, and bandwidth.

Controller type	K_p	K_i	ξ	ω_n	$B.W$
d-axis stator current	1.2	3.8	0.703	206.799	208
q-axis stator current	3.6	10	0.696	146.696	149

5. Experimental Setup and Results

A three-phase, 220 V, 0.75 kW, Y-connected, standard surface-mounting PMSM was used as the controlled plant for experimentation and to confirm the effectiveness of the proposed speed estimation VC MRAS PMSM drive using GA to design the speed controller. In a running cycle, the speed command was designed as follows: forward direction acceleration from $t = 0$ to $t = 1$ s; forward direction steady-state running over $1 \le t \le 6$ s; forward direction braking to reach zero speed at $6 \le t \le 7$ s intervals; reverse direction acceleration from $t = 7$ to $t = 8$ s; reverse direction steady-state running over $8 \le t \le 13$ s; reverse direction braking to reach zero speed at $13 \le t \le 14$ s intervals.

The simulated and experimental responses with a 3 N-m load for the reversible steady-state speed command of 2000 rev/min are respectively shown in Figs. 9 and 10. Each figure contains

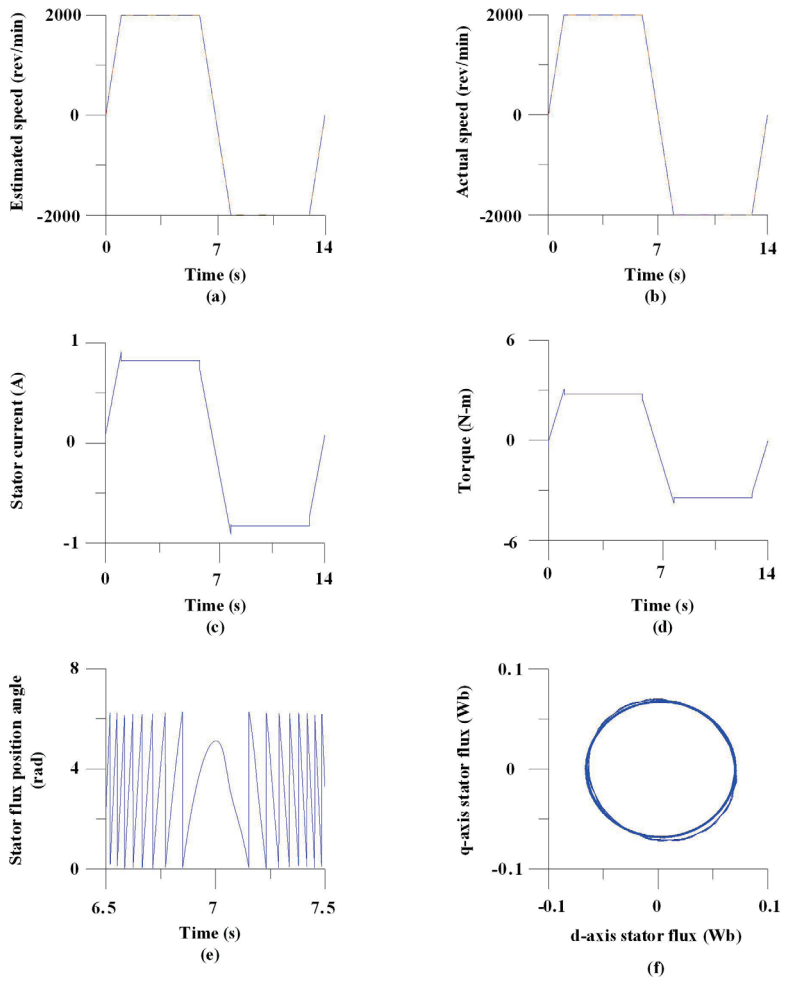

Fig. 9. (Color online) Simulated responses of the proposed speed estimation VC MRAS PMSM drive using GA with 3 N-m load for reversible steady-state speed command of 2000 rev/min. (a) Estimated rotor speed, (b) actual rotor speed, (c) stator current, (d) electromagnetic torque, (e) stator flux position angle, and (f) stator flux locus.

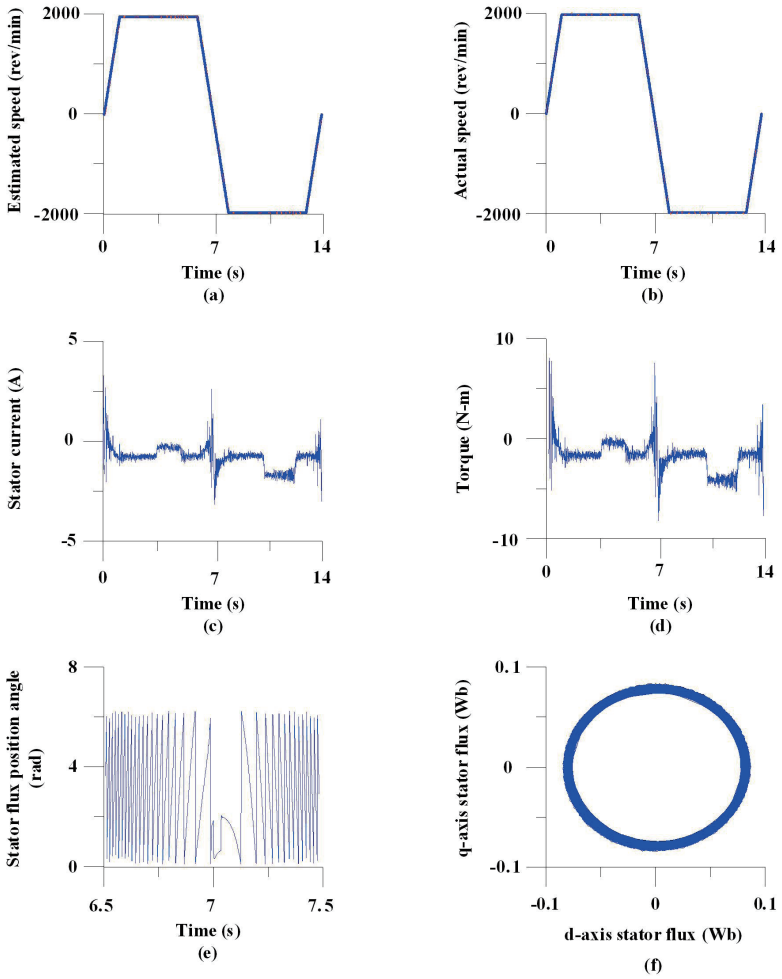

Fig. 10. (Color online) Experimental responses of the proposed speed estimation VC MRAS PMSM drive using GA with 3 N-m load for reversible steady-state speed command of 2000 rev/min. (a) Estimated rotor speed, (b) actual rotor speed, (c) stator current, (d) electromagnetic torque, (e) stator flux position angle, and (f) stator flux locus.

six responses: (a) command (dashed line) and estimated (solid line) rotor speed, (b) command (dashed line) and actual (solid line) rotor speed, (c) stator current, (d) electromagnetic torque, (e) stator flux position angle, and (f) stator flux locus (q-axis vs d-axis).

According to the results of the simulated and experimental tests in reversible transient and steady-state operations, the developed MRAS could accurately estimate the rotor speed, and the designed speed controller could quickly adjust the reversible transient and steady-state response under a load condition. Furthermore, the saw-tooth stator flux position angle and circular stator flux locus confirmed the exact coordinate transformation to be achieved.

6. Conclusions

An adaptive rotor speed estimation scheme was developed to achieve speed estimation for VC PMSM drives. The decoupled VC PMSM drive was established using the stator voltage and current. An MRAS was used to develop an estimated rotor speed scheme based on the reactive power of a PMSM. The designed GA speed controller quickly adjusted the reversible transient and steady-state response under a load condition. The three-phase stator currents for implementing the adaptive speed estimation method of the VC PMSM drive were provided by Hall effect current sensors. The simulation and experimental results confirmed the promising performance of the proposed speed estimation method for a VC PMSM drive using GA.

References

1 Y. C. Luo, S. H. Pei, Y. P. Kuo, and C. T. Tsai: Sens. Mater. **32** (2020) 1851. https://doi.org/10.18494/SAM.2020.2480
2 W. Sun, Y. Yu, G. Wang, B. Li, and D. Xu: IEEE Trans. Power Electron. **31** (2016) 2609. https://doi.org/10.1109/TPEL.2015.2440373
3 W. Xu, Y. Jiang, C. Mu, and F. Blaabjerg: IEEE Trans. Power Electron. **34** (2019) 565. https://doi.org/10.1109/TPEL. 2018.2822769
4 W. Xu, L. Wang, Y. Liu, and F. Blaabjerg: CES Trans. Elec. Mach. Syst. **3** (2019) 151. https://doi.org/10.30941/CESTEMS.2019.00021
5 A. T. Popovici, A. Onea, and A. Barleanu: Proc. 2019 23rd Int. Conf. System Theory, Control Computing (ICSTCC 2019) 379–384. https://doi.org/10.1109/ICSTCC.2019.8885664
6 S. Bose, M. R. Islam, T. Islam, and M. A. Rafiq: Proc. 2017 3rd Int. Conf. Electrical Information Communication Technology (EICT 2017) 1–5. https://doi.org/10.1109/EICT.2017.8275175
7 J. M. Lazi, Z. Ibrahim, S. N. M. Isa, A. M. Razali, Z. Rasin, and N. Kamisman: Proc. IEEE Power Energy (PE 2016) 540–545. https://doi.org/10.1109/PECON.2016.7951620
8 G. Zhang, G. Wang, D. Xu, and N. Zhao: IEEE Trans. Power Electron. **31** (2016) 1450. https://doi.org/10.1109/TPEL.2015.2424256
9 W. Zine, Z. Makni, E. Monmasson, L. Idkhajine, and B. Condamin: IEEE Trans. **14** (2018) 1942. https://doi.org/10.1109/TII.2017.2765398
10 X. Li and R. Kennel: IEEE Trans. Ind. Electron. **68** (2021) 2856. https://doi.org/10.1109/TIE.2020.2977568
11 N. K. Quang, N. T. Hieu, and Q. P. Ha: IEEE Trans. Ind. Electron. **61** (2014) 6574. https://doi.org/10.1109/TIE.2014.2320215
12 R. Yildiz, M. Barut, and E. Zerdali: IEEE Trans. Ind. Inform. **16** (2020) 6423. https://doi.org/10.1109/TII.2020.2964876
13 Z. Yin, G. Li, Y. Zhang, J. Liu, X. Sun, and Y. Zhong: IEEE Trans. Power Electron. **32** (2017) 7096. https://doi.org/10.1109/TPEL.2016.2623806
14 Y. Yao, Y. Huang, F. Peng, and J. Dong: IEEE Trans. Power Electron. **35** (2020) 7341. https://doi.org/10.1109/TPEL.2019.2957058
15 M. Moradian, J. Soltani, A. N. Khodabakhsh, and G. R. A. Markadeh: IEEE Trans. Ind. Inform. **15** (2019) 205. https://doi.org/10.1109/TII.2018.2808521
16 S. S. Badini and V. Verma: IEEE Trans. Ind. Appl. **56** (2020) 6536. https://doi.org/10.1109/TIA.2020.3025265
17 O. C. Kivanc and S. B. Ozturk: IEEE Trans. Ind. Mechatr. **23** (2018) 1326. https://doi.org/10.1109/TMECH.2018.2817246
18 C. H. Liu: Control of AC Electrical Machines (Tunghua, Taipei, 2008) 4th ed., Chap. 5 (in Chinese).
19 Y. C. Luo, Y. C. Ji, C. H. Lin, and W. C. Pu: Sens. Mater. **33** (2021) 345. https://doi.org/10.18494/SAM.2021.3018
20 Z. Jin, W. Jianjing, Z. Huajun, and Y. Wei: Proc. 2011 6th IEEE Conf. Industrial Electronics Applications (ICIEA 2011) 913–918. https://doi.org/10.1109/ICIEA.2011.5975717
21 I. Bahri, A. Maalouf, L. Idkhajine, and E. Monmasson: Proc. 2011 Symp. Sensorless Control Electrical Drives (SLED 2011) 13–18. https://doi.org/10.1109/SLED.2011.6051539